Stability of wall modes in fluid flow past a flexible surface

V. Shankar and V. Kumaran[a]

Department of Chemical Engineering, Indian Institute of Science, Bangalore 560 012, India

The stability of wall modes in fluid flow past a flexible surface is analyzed using asymptotic and numerical methods. The fluid is Newtonian, while two different models are used to represent the flexible wall. In the first model, the flexible wall is modeled as a spring-backed, plate-membrane-type wall, while in the second model the flexible wall is considered to be an incompressible viscoelastic solid of finite thickness. In the limit of high Reynolds number (Re), the vorticity of the wall modes is confined to a region of thickness $O(\mathrm{Re}^{-1/3})$ in the fluid near the wall of the channel. An asymptotic analysis is carried out in the limit of high Reynolds number for Couette flow past a flexible surface, and the results show that wall modes are always stable in this limit if the plate-membrane wall executes motion purely normal to the surface. However, the flow is shown to be unstable in the limit of high Reynolds number when the wall can deform in the tangential direction. The asymptotic results for this case are in good agreement with the numerical solution of the complete governing stability equations. It is further shown using a scaling analysis that the high Reynolds number wall mode instability is independent of the details of the base flow velocity profile within the channel, and is dependent only on the velocity gradient of the base flow at the wall. A similar asymptotic analysis for flow past a viscoelastic medium of finite thickness indicates that the wall modes are unstable in the limit of high Reynolds number, thus showing that the wall mode instability is independent of the wall model used to represent the flexible wall. The asymptotic results for this case are in excellent agreement with a previous numerical study of Srivatsan and Kumaran. © *2002 American Institute of Physics.* [DOI: 10.1063/1.1481055]

I. INTRODUCTION

The dynamics of fluid flow past flexible solid surfaces is qualitatively different from that of rigid surfaces because of the coupling between the fluid and wall dynamics, and the elasticity of the surface could affect the fluid flow. In particular, this coupling could influence the transition from laminar to turbulent flow in such systems. Experiments conducted by Krindel and Silberberg[2] in a gel-walled tube indicate that there is an anomalous drag force at Reynolds numbers (Re) as low as about 600, and the authors concluded that this is due to a transition to a turbulent flow at a Reynolds number which is far lower than the critical Reynolds number for the flow through a rigid tube (around 2100). The transition Re was found to depend on the elasticity of the wall in addition to the fluid properties indicating that the wall dynamics plays a significant role in the transition events. Motivated by these experimental results, there has been a renewed interest in the recent years in the understanding of the stability of fluid flow through flexible tubes and channels.[1–8] These studies have modeled the flexible wall as a viscoelastic continuum of finite thickness, and have used the governing equations for an elastic solid modified to include viscous effects. A summarizing discussion on the results obtained in these theoretical studies is provided in Shankar and Kumaran.[7] Recent experimental studies[9] further confirm the presence of qualitatively new instabilities at low Re in flow past flexible surfaces.

There have been a large number of other studies, motivated by drag reduction in marine and aerospace applications,[10–17] which have studied the stability problem by modeling the flexible wall to be a thin spring-backed plate membrane which executes purely normal motion. Most of these studies were performed in the high Reynolds number limit, where fluid inertial forces are dominant. At high Reynolds number, the Tollmien–Schlichting instability (TSI) is modified owing to the flexibility of the wall. Benjamin[10] extended the classical stability theory of Tollmien and Schlichting,[18] and showed that a flexible nondissipative wall tends to stabilize the TSI, which is the destabilizing mechanism in flow past rigid surfaces. In addition, Benjamin[10] and Landahl[11] pointed out that there is an additional mode of instability that could exist in an inviscid flow, which was termed the flow-induced surface instability (FISI). Carpenter and Garrad[12,13] analyzed the stability of Blasius flow over a compliant plate, in which they considered both TSI and FISI. The TSI was analyzed numerically, while FISI was analyzed using both analytical and numerical methods. These studies concluded that the wall flexibility usually stabilizes the flow in the boundary layer and increases the Reynolds number at which transition to turbulence occurs. Carpenter and Gajjar[16] used a triple-deck asymptotic analysis to study the FISI when the critical layer and the wall layer are well separated. Carpenter and Morris[19] analyzed the effect of anisotropic wall compliance on the stability of Blasius boundary layer flow past flexible surface modeled as a spring-backed wall. Unlike the earlier studies of Carpenter and co-workers, this study

[a]Electronic mail: kumaran@chemeng.iisc.ernet.in

included both normal and tangential motion in the plate-membrane wall. However, the normal and tangential displacements were simply related by a constant factor, corresponding to the inclination of the springs. Larose and Grotberg[15] studied the stability of developing flow in a compliant channel using both long-wave asymptotic analysis and numerical methods. They found a long-wave instability which was not observed in previous channel studies, and this instability was stabilized by increasing the elastance of the wall. Their wall model included both normal and tangential wall displacements. Davies and Carpenter[14] studied the stability of the plane-Poiseuille flow in a compliant channel. This study modeled the compliant walls as spring-backed plates with only normal wall motion. This study analyzed the interconnected behavior of FISI and TSI using both asymptotic and numerical methods, and found that if the compliant wall properties are selected to give a significant stabilizing effect on TSI, the onset of FISI could be severely affected.

The present study addresses the stability of wall modes in a flexible channel using a combination of asymptotic and numerical methods. Wall modes are a class of solutions in the high Reynolds number limit where the vorticity in the fluid is confined to a layer near the wall of the channel (referred henceforth as the wall layer) of thickness $O(\text{Re}^{-1/3})$ smaller than the radius of the channel. The damping rate of these modes is $O(\text{Re}^{-1/3})$ smaller than the strain rate in the fluid. These modes were first studied by Corcos and Sellers[20] and Gill[21] for the case of Hagen–Poiseuille flow in a rigid tube, and these asymptotic studies showed that wall modes are always stable in a rigid tube. Since the vorticity in the fluid is confined near the wall of the channel, the elasticity of the wall can affect the stability of the wall modes in the case of fluid flow through flexible tubes and channels. The stability of wall modes in a flexible tube was analyzed using an asymptotic analysis in the high Reynolds number limit by Kumaran.[8] This analysis mainly focused on the regime Re ≥ 1, and $\Lambda \equiv \text{Re}^{1/3}(G/\rho V^2) \sim 1$. Here, Re$\equiv RV\rho/\eta$ is the Reynolds number, ρ, η are, respectively, the density and viscosity of the Newtonian fluid, V is the maximum velocity of the Hagen–Poiseuille flow, G is the shear modulus of the wall material, and R is the radius of the flexible tube. An asymptotic analysis in the small parameter $\text{Re}^{-1/3}$ was used to determine the growth rate, which showed that there are multiple solutions. In the limit $\Lambda \to \infty$, which corresponds to elastic stresses in the wall very large compared to viscous stresses in the fluid (i.e., the rigid tube limit), the solutions to the growth rate converged to the solutions of Gill[21] for the case of wall modes in a rigid tube. In the opposite limit of $\Lambda \to 0$, which corresponds to a wall with very small elasticity, the growth rates were again found to be stable. The transition from $\Lambda \gg 1$ to $\Lambda \ll 1$ was found to be smooth. However, there is one mode in the limit $\Lambda \ll 1$ in a flexible tube whose growth rate does not converge to any of the rigid tube modes, but the frequency of this mode diverges as Λ in the limit of a rigid tube ($\Lambda \to \infty$), and the decay rate was found to decrease as $\Lambda^{-1/2}$ in the limit $\Lambda \to \infty$. It was then concluded that this represents the least stable wall mode in a flexible tube.[8]

This least stable wall mode in a flexible tube, which is absent in the case of flow in a rigid tube, was continued numerically to the $\Lambda \ll 1$ regime in Ref. 6. That study showed that this particular mode becomes *unstable* when Λ was decreased below a transition value at a given Re, with Re ranging between 1000 and 10 000. The neutral stability curves for this unstable mode was obtained using a numerical continuation scheme, and the Reynolds number for neutral modes was determined as a function of the parameter Σ. The parameter $\Sigma \equiv \rho G R^2/\eta^2$, is a flow-independent quantity which is proportional to the shear modulus G of the flexible tube. The numerical results revealed that the Re for neutral modes decreases proportional to $\Sigma^{1/2}$ in the limit $\Sigma \ll 1$, and shows rather complex behavior in the intermediate regime. In the limit $\Sigma \gg 1$, the transition Reynolds number increases proportional to Σ^α, where α was found to be between 0.7 and 0.75. More recently, the present authors have shown[17] that the numerical results of Refs. 6 and 8 can be obtained by an asymptotic analysis of wall modes in the parameter regime Re$\sim \Sigma^{3/4}$.

The instabilities analyzed in previous studies[12–16] on flow past compliant walls are qualitatively different from the above wall mode instability for the following reasons.

(1) The growth rate for unstable wall modes is $O(\text{Re}^{-1/3})$ smaller than the strain rate of the base flow, while the growth rate for inviscid FISI modes is of the same order as the strain rate of the base flow.

(2) The flow structure of the unstable modes is different in the limit of high Reynolds number for the two instabilities: for wall modes the thickness of the boundary layer $\delta \sim \text{Re}^{-1/3}$ while for inviscid FISI modes $\delta \sim \text{Re}^{-1/2}$.

(3) The critical Reynolds number for the instability to occur scales differently with the nondimensional wall elasticity: Re$\sim \Sigma^{3/4}$ for wall modes, while Re$\sim \Sigma^{1/2}$ for inviscid FISI modes.

(4) In most of the previous studies,[12–16] the shear stress condition at the interface is subdominant, and the instability is primarily determined by normal velocity and stress conditions at the interface. Whereas, as will be shown below, in the present analysis of wall modes the shear stress condition at the interface proves to be crucial in causing the instability.

(5) As demonstrated in this paper, the wall mode instability can exist only in the presence of a tangential deformation in the wall, while the instabilities analyzed in Refs. 12–16 can occur even in the absence of tangential wall deformation.

Consequently, it is of interest to determine the stability of wall modes in fluid flow past a compliant wall, and this is the main objective of the present study. Two different models are used in the present study to represent the flexible wall in order to demonstrate that the unstable wall modes are independent of the wall model used to represent the wall medium. An asymptotic analysis is carried out in Sec. II for the case of stability of Couette flow past a spring-backed wall used in previous studies on stability of flow past flexible surfaces (see, for example, Refs. 14 and 15). In this analysis,

it is shown that the high Reynolds number wall modes are *stable* in the absence of tangential wall motion in the spring-backed wall. However, when tangential motion is introduced in the spring-backed wall model, the wall modes are shown to be unstable in the limit of high Reynolds number. This is contrary to the conventional expectation that the tangential wall motion will be subdominant in the limit of $\text{Re} \gg 1$, because it is reasonable to approximate the fluid dynamics by the inviscid governing equations, and the tangential velocity and stress boundary conditions cannot be satisfied by the inviscid velocity field.

The results of the present asymptotic analysis are in good agreement with the results from a full numerical solution of the governing stability equations. In Sec. III, a similar asymptotic analysis is carried out for the case of Couette flow past a viscoelastic solid in the limit of high Re, and it is shown that the earlier numerical results of Srivatsan and Kumaran[1] are the unstable wall modes predicted by the present study. More importantly, the asymptotic analysis of wall modes in fluid flow past spring-backed walls indicates that the unstable wall modes predicted by the present study should exist in any high Re flow past flexible solid surfaces irrespective of the details of the base flow velocity profile. The only essential feature that the base flow profile should satisfy is that base flow velocity is zero at the wall and should posses a finite velocity gradient at the wall. Since most of the commonly encountered laminar shear flows such as the Couette flow, plane-Poiseuille flow and the Blasius boundary layer flow satisfy this criterion, the high Reynolds number unstable wall modes predicted in this paper are likely to be a generic feature of fluid flow past flexible solid surfaces. As revealed by the asymptotic analysis, an essential ingredient for the present instability is that the flexible surface should be capable of undergoing deformations in the tangential direction—a criterion normally satisfied by realistic flexible (isotropic) solid surfaces such as polymer gels. Consequently, flexible wall models such as spring—backed walls with purely normal wall motion[14] will not capture this instability. Thus the present study shows that inclusion of tangential wall motion in the flexible medium can give rise to a qualitatively new instability in the limit of high Reynolds number where the viscous stresses in the fluid are confined within a thin layer of thickness $O(\text{Re}^{-1/3})$ near the flexible wall, and these instabilities are absent for flexible wall models which exhibit only purely normal wall motion.

The rest of this paper is organized as follows. Sec. II presents the asymptotic analysis and corresponding numerical results for the stability of Couette flow past a spring backed surface in the limit of high Re. Details of this asymptotic analysis are given in Appendix A. Section III demonstrates that a similar instability exists in fluid flow past a viscoelastic material of finite thickness. Numerical results are presented alongside, and it is shown that the asymptotic and numerical results are in good agreement. The salient conclusions of the present study are provided in Sec. IV.
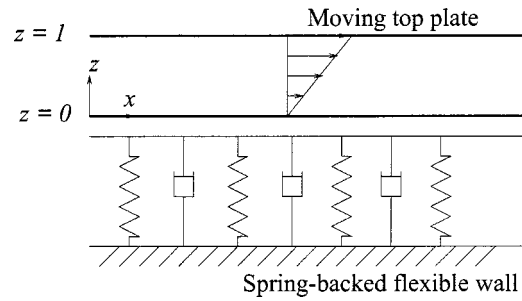

FIG. 1. Schematic diagram showing the configuration and coordinate system considered in Sec. II.

II. WALL MODES IN COUETTE FLOW PAST A SPRING-BACKED WALL

In this section, an asymptotic analysis is carried out for the stability of Couette flow past a spring-backed plate membrane wall. The system consists of a fluid of thickness R which is bounded at $z^* = R$ by a rigid surface moving at a constant velocity V, as shown in Fig. 1. In what follows, quantities with a superscript * are dimensional, while dynamical quantities without a superscript are dimensionless. At the lower boundary $z^* = 0$, there is a plate-membrane wall,[15,14] which is a spring-backed plate deformable both in the horizontal and vertical directions. The displacement in the horizontal and vertical directions, denoted, respectively, by u_x^* and u_z^*, represent the deviation of the material points in the wall material from their equilibrium positions. In the previous studies, a constitutive equation of the following type,

$$(M^* \partial_t^{*2} + D_n^* \partial_t^* + B^* \partial_x^{*4} - T^* \partial_x^{*2} + K^*) u_z^* = n_i \tau_{ij}^* n_j, \tag{1}$$

has been used for the normal displacement of the membrane (u_z^*). Here τ_{ij}^* is the total stress tensor in the fluid and n_i is the unit normal to the flexible surface. In the present study, the above condition is augmented by another relation between the tangential stress and the tangential displacement:[15]

$$(M^* \partial_t^{*2} + D_t^* \partial_t^* - E^* \partial_x^{*2}) u_x^* = t_i \tau_{ij}^* n_j. \tag{2}$$

In the above equations (1) and (2), $n_i \tau_{ij}^* n_j$ and $t_i \tau_{ij}^* n_j$ are, respectively, the normal and tangential fluid stress at the interface, and t_j is the unit vector tangential to the flexible surface. D_n^* is the normal wall damping coefficient, D_t^* is the tangential wall damping coefficient, B^* is the flexural rigidity of the plate, T^* is the longitudinal tension per unit width, K^* is the spring stiffness of the membrane, E^* is the bending stiffness of the membrane, M^* is the mass per unit area of the membrane, x^* is the Cartesian coordinate along the wall, z^* is the direction normal to the wall, $\partial_x^* \equiv \partial/\partial x^*$, t^* is the dimensional time variable and $\partial_t^* \equiv \partial/\partial t^*$. The equations describing the wall dynamics are nondimensionalized in the following manner. Lengths are scaled by R the thickness of the fluid layer flowing above the membrane, velocities by $(E^*/(\rho R))^{1/2}$, where ρ is the density of the Newtonian fluid flowing above the membrane wall, t^* is scaled by $R(\rho R/E^*)^{1/2}$ and the fluid stresses are

Phys. Fluids, Vol. 14, No. 7, July 2002

Stability of wall modes in fluid flow   2327

scaled by E^*/R. The nondimensional governing equations describing the wall dynamics take the following form:

$$n_i \tau_{ij} n_j = [M \partial_t^2 - T \partial_x^2 + D_{nr} \Gamma \, \mathrm{Re}^{-1} \, \partial_t + B \partial_x^4 + K] u_z, \quad (3)$$

$$t_i \tau_{ij} n_j = [M \partial_t^2 - \partial_x^2 + D_{tr} \Gamma \, \mathrm{Re}^{-1} \, \partial_t] u_x, \quad (4)$$

where the various nondimensional parameters are $M = M^*/(\rho R)$, $D_{nr} = D_n^* R/\eta$, $D_{tr} = D_t^* R/\eta$, $B = B^*/(E^* R^2)$, $T = T^*/E^*$, $K = K^* R^2/E^*$, and $\Gamma = (\rho V^2 R/E^*)^{1/2}$ is the nondimensional velocity of the top plate. Here τ_{ij} is the total stress tensor in the fluid scaled by E^*/R. In the following analysis, we set $D_{tr} = D_{nr} = D_r$ for simplicity and in order to reduce the parameter space to be probed. The boundary conditions at the interface between the fluid and the wall are the continuity of velocities and stresses in the normal and tangential directions. At the upper rigid plate ($z=1$), no-slip boundary conditions are appropriate for both the components of the fluid velocity. The velocity continuity conditions at the membrane surface are

$$v_x = \partial_t u_x, \quad v_z = \partial_t u_z, \quad (5)$$

where v_x and v_z are the horizontal and vertical components of the fluid velocity field at the interface. These boundary conditions are supplemented by the stress balance conditions at the interface (3) and (4). The perturbation to the normal and tangential displacements u_z and u_x in the membrane model are expressed in the form of Fourier modes:

$$u_z = \tilde{u}_z \exp[ik(x - ct)], \quad u_x = \tilde{u}_x \exp[ik(x - ct)]. \quad (6)$$

Here, k is the wave number, c is the complex wave speed of the perturbations, $\tilde{u}_z$ and $\tilde{u}_x$ are, respectively, the Fourier components of the displacements u_z and u_x. The wave speed c is in general a complex quantity, and the flow is temporally unstable if the imaginary part of c is positive. The perturbations to the fluid velocity components are expressed in Fourier modes. The boundary conditions Eqs. (3), (4), and (5) at the interface between the fluid and the wall must be applied at the perturbed position of the interface. However, in the linear stability analysis, the velocity and stress fields due to the mean flow and perturbations at the perturbed interface are expanded in a Taylor series about their values at the unperturbed interface at $z=0$. Only the linear terms in the series expansion are retained and higher-order terms are neglected to obtain the following boundary conditions in which all quantities are evaluated at the unperturbed interface:

$$\tilde{v}_z = -ikc\tilde{u}_z, \quad \tilde{v}_x + \Gamma \tilde{u}_z = -ikc\tilde{u}_x. \quad (7)$$

In this equation, $\tilde{v}_z$ and $\tilde{v}_x$ are the Fourier components of the fluid x and z directional disturbance velocities. The fluid normal and tangential stresses at the perturbed interface are, respectively, given by $n_i \tau_{ij} n_j$ and $t_i \tau_{ij} n_j$. Here, n_j and t_j are, respectively, the unit vectors in the normal and tangential directions to the perturbed interface, τ_{ij} is the fluid stress tensor at the interface which is given by the sum of the mean and perturbation stresses, i.e., $\tau_{ij} = \tau_{ij}^m + \tau_{ij}'$. The stress tensor in the Newtonian fluid, nondimensionalized by E^*/R, is given by $\tau_{ij} = -p\delta_{ij} + \Gamma \, \mathrm{Re}^{-1} (\partial_i v_j + \partial_j v_i)$. The expressions for the unit vectors normal and tangential to the deformed surface, to linear order in the perturbation quantities, are

$$\mathbf{n} = \mathbf{e}_z - \partial_x u_z \mathbf{e}_x, \quad \mathbf{t} = \mathbf{e}_x + \partial_x u_z \mathbf{e}_z. \quad (8)$$

Here $\mathbf{e}_x$ and $\mathbf{e}_z$ are unit vectors in the horizontal (x) and vertical (z) directions, respectively (see Fig. 1). The mean shear stress tensor due to the base flow at the interface is $\Gamma \, \mathrm{Re}^{-1} \mathbf{e}_x \mathbf{e}_z$, where $\mathrm{Re} = RV\rho/\eta$ is the Reynolds number of the flow. Therefore, the normal stress at the perturbed interface $n_i \tau_{ij} n_j$, correct to linear order in perturbation quantities, is

$$\mathbf{n} \cdot \boldsymbol{\tau} \cdot \mathbf{n} = -2\Gamma \, \mathrm{Re}^{-1} \, \partial_x u_z - p_f + 2\partial_z v_z. \quad (9)$$

The term $-2\Gamma \, \mathrm{Re}^{-1} \, \partial_x u_z$ represents the mean stress at the interface due to the variation in the unit normal of the perturbed interface. Therefore, the normal stress boundary condition at the unperturbed interface ($z=0$) is given, to linear order, by

$$-2\Gamma \, \mathrm{Re}^{-1} \, ik\tilde{u}_z + (-\tilde{p}_f + 2\Gamma \, \mathrm{Re}^{-1} \, \partial_z \tilde{v}_z)$$
$$= (-k^2 c^2 M - ikcD_r \Gamma \, \mathrm{Re}^{-1} + Tk^2 + Bk^4 + K)\tilde{u}_z. \quad (10)$$

The tangential stress boundary condition at the unperturbed interface $z=0$ is given by

$$\Gamma \, \mathrm{Re}^{-1}(\partial_z \tilde{v}_x + ik\tilde{v}_z) = (-k^2 c^2 M - ikcD_r + k^2)\tilde{u}_x. \quad (11)$$

The tangential stress boundary condition does not have any contributions from the variation of unit normal in the interface, since these contributions are nonlinear in the perturbation quantities. The governing equations for the fluid motion are the Navier–Stokes equations

$$\partial_i v_i = 0, \quad (\partial_t + v_j \partial_j)v_i = -\partial_i p_f + \mathrm{Re}^{-1} \Gamma \partial_j^2 v_i, \quad (12)$$

where the subscripts i and j represent components of a vector, repeated subscripts represent dot products, $\partial_t \equiv \partial/\partial t$ and $\partial_i \equiv \partial/\partial x_i$. In Eq. (12), v_i and p_f are the nondimensional velocity and pressure fields in the fluid, respectively. In the above equation, $\mathrm{Re} = RV\rho/\eta$ is the Reynolds number of the flow based on the top plate velocity and the width of the channel. In the linear stability analysis, small-amplitude normal mode perturbations are imposed on the fluid velocity field

$$v_i = \bar{v}_x(z)\delta_{ix} + \tilde{v}_i(z)\exp[ik(x - ct)], \quad (13)$$

where $\bar{v}_x(z) \equiv \Gamma z$ is the laminar Couette flow velocity profile whose stability is of interest here.

The above form of perturbations are substituted in the governing equations in the fluid medium, and only the quantities that are linear in the perturbation variables are retained to obtain the governing linear stability equations. The resulting nondimensional equations governing the linear stability of the Couette flow are

$$d_z \tilde{v}_z + ik\tilde{v}_x = 0, \quad (14)$$

$$ik\left[z - \frac{c}{\Gamma}\right]\tilde{v}_x + \tilde{v}_z = -ik\frac{\tilde{p}_f}{\Gamma} + \mathrm{Re}^{-1}(d_z^2 - k^2)\tilde{v}_x, \quad (15)$$

$$ik\left[z - \frac{c}{\Gamma}\right]\tilde{v}_z = -\frac{d_z \tilde{p}_f}{\Gamma} + \mathrm{Re}^{-1}(d_z^2 - k^2)\tilde{v}_z. \quad (16)$$

Here, and in what follows, $d_z = d/dz$. Equations (14)–(16) along with the boundary conditions (7), (10), and (11) com-

plete the specification of the stability problem. It is useful to combine Eqs. (14)–(16) into a single Orr–Sommerfeld-type fourth order differential equation

$$\mathcal{L}_v \mathcal{L}_o \tilde{v}_z = 0, \tag{17}$$

where $\mathcal{L}_o$ is an inviscid operator given by $[d_z^2 - k^2]$ which does not contain viscous effects, and $\mathcal{L}_v$ is a viscous operator $[(z - c/\Gamma) - (ik\,\mathrm{Re})^{-1}\mathcal{L}_o]$ which contains viscous effects. The above fourth order Orr–Sommerfeld equation has four linearly independent solutions, and we write the solution to the governing Eq. (17) as two parts

$$\tilde{v}_i = \tilde{v}_{oi} + \tilde{v}_{vi} \quad (i = x, z), \tag{18}$$

which are defined by $\mathcal{L}_o \tilde{v}_{oz} = 0$ and $\mathcal{L}_v \mathcal{L}_o \tilde{v}_{vz} = 0$. The solution to $\mathcal{L}_o \tilde{v}_{oz} = 0$ contains two of the linearly independent solutions to (17):

$$\tilde{v}_{oz} = A_1 \exp[kz] + A_2 \exp[-kz]. \tag{19}$$

We refer to these two linearly independent solutions as the inviscid solutions since these solutions are independent of Re and consequently are devoid of viscous effects. It is also useful to note that differential equation $\mathcal{L}_o \tilde{v}_{oz} = 0$ is equivalent to formally setting Re^{-1} to zero in Eqs. (14)–(16):

$$d_z \tilde{v}_{oz} + ik \tilde{v}_{ox} = 0, \tag{20}$$

$$ik\left(U - \frac{c}{\Gamma}\right)\tilde{v}_{ox} + \tilde{v}_{oz} = -ik\frac{\tilde{p}_{of}}{\Gamma}, \tag{21}$$

$$ik\left(U - \frac{c}{\Gamma}\right)\tilde{v}_{oz} = -\frac{d_z \tilde{p}_{of}}{\Gamma}. \tag{22}$$

The above equations can be combined to yield $\mathcal{L}_o \tilde{v}_{oz} = 0$. However, as is well known, the viscous terms in the governing equations contain the highest derivatives, and the neglect of these terms converts the momentum equations from second order to first order differential equations. Consequently, it is not possible to satisfy all the boundary conditions required for the original viscous second order differential equations using $\tilde{v}_{oz}$ and $\tilde{v}_{ox}$, and only the normal velocity and stress conditions can be satisfied at the interface.

It is not possible to obtain analytical expressions for the other two linearly independent solutions of Eq. (17), and a high Reynolds number asymptotic analysis is carried out here to determine asymptotic approximations to the other two viscous solutions $\tilde{v}_{vi}$. In the limit of high Reynolds number, viscous effects are $O(\mathrm{Re}^{-1})$ smaller than the fluid inertial stresses in the bulk of the channel, and therefore the other two linearly independent viscous solutions, in which viscous stresses become the same order of magnitude as the inertial stresses, are dominant only near the walls. Consequently, to satisfy the tangential velocity and stress conditions, it is necessary to postulate two viscous wall layers near $z = 0$ and $z = 1$ of thickness δ small compared to the channel width

$$\tilde{v}_{vi} = \tilde{v}_{\mathrm{top},vi} + \tilde{v}_{\mathrm{bot},vi} \quad (i = x, z), \tag{23}$$

where $\tilde{v}_{\mathrm{top},vi}$ and $\tilde{v}_{\mathrm{bot},vi}$ are, respectively, the two linearly independent viscous solutions important near the top ($z = 1$) and bottom ($z = 0$) walls. We restrict attention to the

wall layer at $z = 0$ (the fluid-flexible wall interface; see Fig. 1), since it is shown in Appendix A that the viscous solution near the top rigid plate is not relevant to the determination of the growth rate in the present problem.

The wave speed of wall modes are $O(\mathrm{Re}^{-1/3})$ small compared to the characteristic velocity of the base flow,[6,20,21] and within the present scheme of nondimensionalization, this condition reduces to $c/\Gamma \sim \mathrm{Re}^{-1/3}$, since Γ is the nondimensional maximum velocity of the base velocity profile. In this paper, we further consider the scaling regime $\Gamma \sim \mathrm{Re}^{1/3}$ for the following reason. At the interface between the fluid and flexible wall, the viscous shear stresses and the elastic stresses are of the same order as dictated by the tangential stress continuity condition Eq. (4). The dimensional viscous shear stresses can be estimated to be of the order of $\eta V/(\delta R)$, where V is the dimensional velocity of the top plate, δR is the length scale of variation near the wall (the scaling for small parameter $\delta \sim \mathrm{Re}^{-1/3}$ is derived in Appendix A), and η is the viscosity of the fluid. The dimensional elastic stresses in the elastic wall can be estimated to be of E^*/R [from Eq. (2)]. At the interface, the fluid tangential viscous stresses and the wall elastic stresses balance each other, and hence $E^*/R \sim \eta V/(\mathrm{Re}^{-1/3} R)$, which immediately yields $\Gamma \sim \mathrm{Re}^{1/3}$. Since $\Gamma \sim \mathrm{Re}^{1/3}$ and $c/\Gamma \sim \mathrm{Re}^{-1/3}$ we consider $c \sim O(1)$. Therefore, c is expanded in an asymptotic series

$$c = c^{(0)} + \delta c^{(1)} + \cdots. \tag{24}$$

It is convenient to write $\Gamma = \Gamma_0 \mathrm{Re}^{1/3}$, where Γ_0 is an $O(1)$ quantity. The relation between the thickness of the wall layer δ and Re is determined by a scaling analysis of the x-momentum equation of the fluid (15). In the wall layer, it is appropriate to rescale the z coordinate by $z = \xi \delta$. The base flow velocity profile $U(z) = z$ is then expressed as $U(z) = \xi \delta$ near the fluid-wall interface. The derivatives d_z transform in the wall layer as $d_z = \delta^{-1} d_\xi$ (where $d_\xi = d/d\xi$). The continuity equation (14) then indicates that $\tilde{v}_{\mathrm{bot},vz} = O(\delta)\tilde{v}_{\mathrm{bot},vx}$ in the wall layer, and the fluid velocities are expanded in the following asymptotic series:

$$\tilde{v}_{\mathrm{bot},vx} = \tilde{v}_{\mathrm{bot},vx}^{(0)} + \delta \tilde{v}_{\mathrm{bot},vx}^{(1)} + \cdots,$$

$$\tilde{v}_{\mathrm{bot},vz} = \delta \tilde{v}_{\mathrm{bot},vz}^{(0)} + \delta^2 \tilde{v}_{\mathrm{bot},vz}^{(1)} + \cdots. \tag{25}$$

The scaled governing equations in the wall layer and the outer layer obtained using the above asymptotic expansions, and the solutions to the fluid velocity field in both the layers are provided in Appendix A. It suffices here to write down the fluid velocity fields and the pressure field, obtained by adding the inviscid and viscous eigenfunctions

$$\tilde{v}_z = \delta \tilde{v}_{\mathrm{bot},vz}^{(0)} + \delta^2 \tilde{v}_{oz}^{(0)}, \tag{26}$$

$$\tilde{v}_x = \tilde{v}_{\mathrm{bot},vx}^{(0)} + \delta^2 \tilde{v}_{ox}^{(0)}, \tag{27}$$

$$\tilde{p}_f = \delta \tilde{p}_{of} + \delta^2 \tilde{p}_{\mathrm{bot},vf}^{(0)}, \tag{28}$$

where the expressions for $\tilde{v}_{\mathrm{bot},vz}^{(0)}$ and $\tilde{v}_{\mathrm{bot},vx}^{(0)}$ are given in (A12) and (A13) of Appendix A, the expression for $\tilde{v}_{oz}$ is provided in (A20). There are two unknown constants C_2 and A_1 in Eqs. (A13) and (A20) (see Appendix A), and there are four boundary conditions at the interface ($z = 0$), viz., nor-

mal and tangential velocity continuity and normal and tangential stress continuity conditions, which involve two unknown displacements u_z and u_x. Thus, there are four boundary conditions and four undetermined constants, and the problem is well-specified.

In this section, boundary conditions at the fluid-wall interface are considered for surfaces with and without tangential motion. For the case of membrane walls without tangential motion, $\tilde{u}_x$ is set to zero at $z=0$ and the tangential stress condition (11) is omitted.

A. Plate model with tangential wall motion

The unscaled boundary conditions at $z=0$ for the case where there is tangential wall motion in the plate membrane are given by

$$\tilde{v}_z = -ikc\tilde{u}_z, \tag{29}$$

$$\tilde{v}_x + \Gamma\tilde{u}_z = -ikc\tilde{u}_x, \tag{30}$$

$$\Gamma\,\mathrm{Re}^{-1}(\partial_z\tilde{v}_x + ik\tilde{v}_z)$$
$$= [-Mk^2c^2 - ikcD_r\,\mathrm{Re}^{-1}\,\Gamma + k^2]\tilde{u}_x, \tag{31}$$

$$-2\Gamma\,\mathrm{Re}^{-1}\,ik\tilde{u}_z + (-\tilde{p}_f + 2\Gamma\,\mathrm{Re}^{-1}\,\partial_z\tilde{v}_z)$$
$$= (-k^2c^2M - ikcD_r\,\mathrm{Re}^{-1}\,\Gamma + Tk^2 + Bk^4 + K)\tilde{u}_z. \tag{32}$$

Here, Eqs. (29) and (30) are, respectively, the normal and tangential velocity boundary conditions, and Eqs. (31) and (32) are, respectively, the tangential and normal stress boundary conditions at the interface. Equations (29) and (30) can be used to represent $\tilde{u}_z$ and $\tilde{u}_x$ in terms of $\tilde{v}_z$ and $\tilde{v}_x$ at the interface as follows:

$$\tilde{u}_z = i\tilde{v}_z/(kc), \quad \tilde{u}_x = i\tilde{v}_x/(kc) - \Gamma\tilde{v}_z/(k^2c^2). \tag{33}$$

The above expressions are substituted in the tangential and normal stress conditions (31) and (32). The expansions (25) and (A18) are substituted in the normal stress boundary condition (31), and to leading order in δ, we obtain

$$-\tilde{p}_{of}^{(0)} = \{-k^2c^2M + Tk^2 + Bk^4 + K\}[i\tilde{v}_{vz}^{(0)}/(kc^{(0)})]. \tag{34}$$

Here, the nondimensional model parameters in the curly braces are assumed to be $O(1)$, in the sense that the nondimensional quantities do not scale with the small parameter δ. Thus, the scaling assumption made in Eq. (A17) for the inviscid contribution to the fluid pressure is consistent with the above boundary condition. It can further be verified from the inviscid x-momentum equation (21) that the inviscid contributions to the fluid velocities are $O(\delta^2)$, since $\tilde{p}_{of} \sim O(\delta)$. This is in agreement with the scaling assumptions made in Eq. (A17) for the inviscid velocity components $\tilde{v}_{oz}$ and $\tilde{v}_{ox}$. The expansions (25) and (A18) are substituted in the tangential stress boundary condition (31), and we obtain to $O(\delta)$:

$$k^2(1 - M(c^{(0)})^2 - 2\delta Mc^{(0)}c^{(1)})\left[\frac{i\tilde{v}_{vx}^{(0)}}{kc^{(0)}} - \frac{\Gamma_0\tilde{v}_{vz}^{(0)}}{k^2(c^{(0)})^2}\right]$$

$$= \delta\Gamma_0\,d_\xi\tilde{v}_{vx}^{(0)}. \tag{35}$$

The inviscid normal velocity $\tilde{v}_{oz}$ does not enter into the above equation since it is $O(\delta^2)$ smaller than the tangential velocity $\tilde{v}_{\mathrm{bot},vx}$ in the wall layer. To leading order in δ, the above equation yields

$$k^2[1 - M(c^{(0)})^2] = 0, \tag{36}$$

which can be solved to give the leading order wave speed $c^{(0)} = \sqrt{1/M}$. Since M is a positive real quantity, this result implies that the perturbations are neutrally stable in the leading approximation. The first correction to the above equation (35) can be readily obtained as

$$-2Mc^{(1)}[ikc^{(0)}\tilde{v}_{\mathrm{bot},vx}^{(0)} - \Gamma_0\tilde{v}_{\mathrm{bot},vz}^{(0)}] = \Gamma c^{(0)}\,d_\xi\tilde{v}_{\mathrm{bot},vx}^{(0)}, \tag{37}$$

which yields an expression for $c^{(1)}$,

$$c^{(1)} = \frac{-\Gamma_0 c^{(0)}}{2M}\left[\frac{d_\xi\tilde{v}_{\mathrm{bot},vx}^{(0)}}{ikc^{(0)}\tilde{v}_{\mathrm{bot},vx}^{(0)} - \Gamma_0\tilde{v}_{\mathrm{bot},vz}^{(0)}}\right]. \tag{38}$$

In the above expression, all the dynamical quantities in the bottom wall layer must be evaluated at $z = \xi = 0$, i.e., at the fluid-wall interface, and expressions (A12) are derived in the preceding section for the wall layer quantities $\tilde{v}_{\mathrm{bot},vx}^{(0)}$, $\tilde{v}_{\mathrm{bot},vz}^{(0)}$. This calculation shows that $c^{(1)}$ is a complex quantity, and the imaginary part of $c^{(1)}$ is set to zero to obtain the scaled velocity Γ_0 required for neutrally stable modes. Thus, the present asymptotic analysis shows that the high Reynolds number wall modes in Couette flow past a spring-backed plate membrane are unstable if the membrane has tangential deformations. Interestingly, the asymptotic expression for $c^{(1)}$ (38) indicates that the high Reynolds number wall mode instability is independent of the parameters T, K, and B that occur in the normal stress balance, in the limit of high Reynolds number. The instability depends only on the dimensionless parameter $\Gamma_0 = \Gamma\,\mathrm{Re}^{-1/3}$ [$\Gamma = (\rho V^2 R/E^*)^{1/2}$ is the nondimensional velocity of the top plate] and the dimensionless mass per unit area of the membrane M.

The above asymptotic results are verified by numerically solving the complete equations governing the stability (14)–(16) along with the boundary conditions (29)–(32). The numerical method used to solve the fluid equations is identical to the one used in Ref. 1 for Couette flow past a viscoelastic medium, and a Newton–Raphson method is used to solve the characteristic equation that arises from the boundary conditions. The results from the numerical solution are compared with the asymptotic results for high Reynolds number wall modes in Figs. 2 and 3. Figure 2 shows the comparison between asymptotic and numerical results for different values of M (the nondimensional mass per area of the plate membrane). In this figure, the neutral stability results are plotted in the Re–Σ plane, where $\Sigma = \rho RE^*/\eta^2 \equiv (\mathrm{Re}/\Gamma)^2$ is a flow-independent nondimensional quantity characterizing the elasticity of the membrane wall. This figure shows that the numerical results are accurately captured by the asymptotic analysis. Figure 3 shows the neutral stability curves obtained from the asymptotic and the full numerical solution for different values of T and K. This figure shows that all the neutral curves approach each other at high Reynolds number and they all converge to the asymptotic result. This numerical
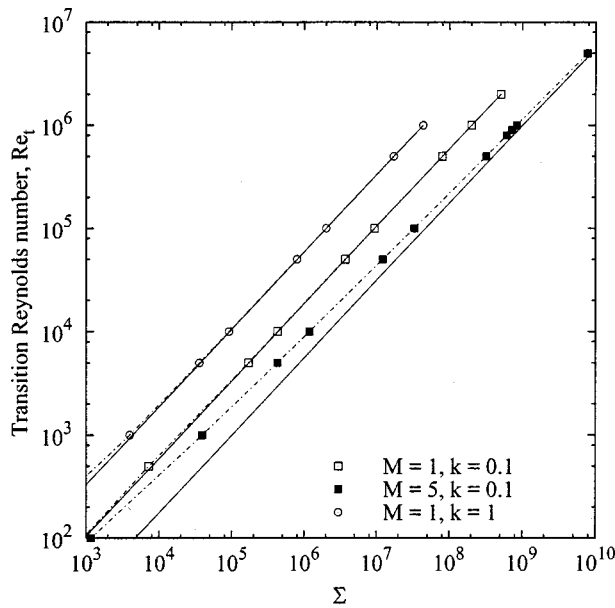
FIG. 2. Comparison of the asymptotic results (solid lines) obtained from the high Re analysis with the numerical results (dotted lines with symbols) obtained from the solution of the complete governing equations: For spring-backed walls with tangential motion. $T=1$, $K=1$, $D_r=0$, $B=10^{-3}$ for all the cases plotted.

result is in agreement with the prediction of the asymptotic analysis that at high Re the instability is independent of the parameters K and T occurring in the normal stress balance at the interface. Thus, the results from the numerical solution of the complete governing equations and boundary conditions are in good agreement with the asymptotic results.
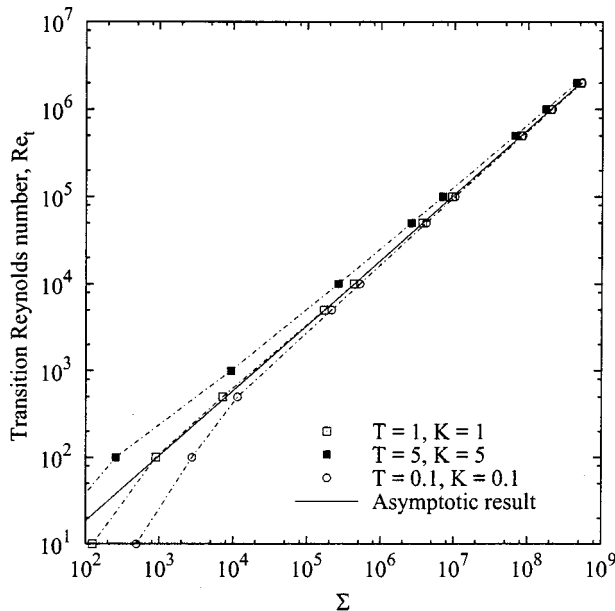

FIG. 3. Comparison of the asymptotic results (solid line) obtained from the high Re analysis with the numerical results (dotted lines with symbols) obtained from the solution of the complete governing equations for spring-backed walls with tangential motion: figure illustrates that the neutral curve is independent of K and T at high Reynolds number. $M=1$, $k=0.1$, $D_r=0$, $B=10^{-3}$ for all the cases plotted.

Though the present instability is specifically demonstrated above for the case of Couette flow past a spring-backed wall, it is argued below that the instability is expected to be independent of the actual nature of the base flow velocity profile. The instability just depends on the fact that the base velocity should be zero at the wall, and has finite velocity gradient at the wall. Since most of the commonly encountered viscous shear flows such as Couette flow, plane-Poiseuille flow and the boundary layer flow exhibit this characteristic, the high Re wall modes predicted in this paper are likely to be a generic feature in fluid flow past flexible solid surfaces. This can be demonstrated by a simple scaling analysis of the Orr–Sommerfeld (OS) equation for a general base flow profile $U(z)$. The OS equation for stability of the laminar flow $U(z)$ is given by

$$\left(U-\frac{c}{\Gamma}\right)(\partial_z^2-k^2)\tilde{v}_z-U''\tilde{v}_z=\frac{1}{ik\,\text{Re}}(\partial_z^2-k^2)^2\tilde{v}_z. \quad (39)$$

Here $\tilde{v}_z$ is the normal velocity of the perturbations, z is the normal direction, $U(z)$ is the base flow in the x direction, and $U''(z)$ is the second derivative of $U(z)$ with respect to z. Note that $U(z)=z$ and U'' was identically zero for the case of Couette flow considered in the above asymptotic analysis. Let $z=0$ be the location of the unperturbed flexible wall. As discussed before, for wall modes, it is necessary to introduce a new variable such that $\delta\xi=z$, where $\delta=\text{Re}^{-1/3}$. Since we are interested in a region very near the wall, the base flow velocity $U(z)$ can be Taylor expanded as [after noting that $U(z=0)=0$]: $U(z)=U'_{\text{wall}}z=U'_{\text{wall}}\xi\delta$, where U'_{wall} is the gradient of the mean velocity profile at the wall. Thus the base flow velocity in the wall layer is $O(\delta)$. As mentioned before, the ratio c/Γ is $O(\delta)$ for wall modes. In the wall layer $\partial_z^2\sim\delta^{-2}\partial_\xi^2$. Therefore, the first term on the left-hand side of (39) is $O(\delta^{-1}\tilde{v}_z)$. The order of magnitude of the term $U''\tilde{v}_z$ in (39) is estimated by Taylor expanding U'' about $z=0$, and to leading order this yields U''_{wall}, which is an $O(1)$ quantity. Thus the order of magnitude of the second term is $O(\tilde{v}_z)$. Consequently, the term $U''\tilde{v}_z$ in the OS equation is smaller by $O(\delta)$ compared to the first term $(U-c/\Gamma)(\partial_z^2-k^2)\tilde{v}_z$ in the wall layer. Therefore, the term $U''(z)$, which is nonzero for a general viscous shear flow, is subdominant in the wall layer. The first correction to the wave speed $c^{(1)}$ is also independent of the inviscid fluid velocity $\tilde{v}_{oz}$, since the inviscid normal velocity $\tilde{v}_{oz}$ is $O(\delta)$ smaller than the viscous normal velocity of the fluid $\tilde{v}_{\text{bot},vz}$ in the wall layer. Consequently, the first correction to the growth rate $c^{(1)}$ is independent of the functional form of the base flow velocity profile. As a result, the wall mode instability predicted in the present study for the case of a Couette flow past a flexible surface is expected to be present in any viscous shear flow which has zero velocity at the wall and a finite velocity gradient near the wall.

B. Plate model without tangential wall motion

In this section, we carry out an asymptotic analysis, similar to one in the preceding section, for the case where there is no tangential wall motion. The equation governing the normal wall motion given in (1) is supplemented by the

normal and tangential velocity continuity conditions, while the tangential stress condition is omitted. The tangential velocity condition is employed here with $u_x = 0$. In Sec. II A, the constitutive equation for the tangential wall motion (2) was used to nondimensionalize various dynamical quantities. In the absence of the tangential stress condition, the various dynamical quantities are nondimensionalized with different scales in this section. The fluid stresses are scaled by K^*R, velocities are scaled by $(K^*R/\rho)^{1/2}$, time is scaled by $(K^*/(\rho R))^{-1/2}$ and the nondimensional top plate velocity is given by $\Gamma \equiv (\rho V^2/(K^*R))^{1/2}$. The nondimensional form of (1) is given by

$$n_i \tau_{ij} n_j = [M \partial_t^2 - T \partial_x^2 + D_{nr} \Gamma \, \mathrm{Re}^{-1} \, \partial_t + B \partial_x^4 + 1] u_z, \tag{40}$$

where the various nondimensional parameters are $M = M^*/(\rho R)$, $D_{nr} = D_n^* R/\eta$, $B = B^*/(K^*R^4)$, $T = T^*/(K^*R^2)$. The nondimensional boundary conditions in terms of Fourier modes for a plate wall model without tangential wall motion are

$$\tilde{v}_z = -ikc\tilde{u}_z, \quad \tilde{v}_x + \Gamma \tilde{u}_z = 0, \tag{41}$$

$$-2\Gamma \, \mathrm{Re}^{-1} \, ik\tilde{u}_z + (-\tilde{p}_f + 2\Gamma \, \mathrm{Re}^{-1} \, \partial_z \tilde{v}_z)$$
$$= (-k^2 c^2 M - ikc D_r \Gamma \, \mathrm{Re}^{-1} + Tk^2 + Bk^4 + 1)\tilde{u}_z. \tag{42}$$

As discussed in the preceding section, the characteristic scaling for the wave speed for wall modes is given by $c/\Gamma \sim \mathrm{Re}^{-1/3}$. In this section, we again consider $\Gamma \sim \mathrm{Re}^{1/3}$ and $c \sim O(1)$ so that $c/\Gamma \sim \mathrm{Re}^{-1/3}$. It can be verified that the other alternative scaling $c \sim \mathrm{Re}^{-1/3}$ and $\Gamma \sim O(1)$ does not allow for nontrivial solutions in the limit of high Re. After letting $c \sim O(1)$ and $\Gamma \sim \mathrm{Re}^{1/3}$, the rest of the scaling arguments presented in the preceding section for the various dynamical quantities in the fluid carry over for the present case as well. In particular, the inviscid fluid velocity components $\tilde{v}_{oz}$ and $\tilde{v}_{ox}$ are $O(\delta^2)$ small compared to the viscous wall layer velocity field $\tilde{v}_{\mathrm{bot},vx}$, in order to satisfy the normal stress condition (42), for reasons similar to that mentioned in the preceding section for plate model with tangential motion. The normal velocity continuity (41) can be used to eliminate $\tilde{u}_z$ in terms of $\tilde{v}_z$ as $\tilde{u}_z = i\tilde{v}_z/(kc)$ and this is substituted in the normal stress condition and the tangential velocity condition. The tangential velocity condition (41) then becomes, after noting $\Gamma_0 = \Gamma \, \mathrm{Re}^{-1/3}$:

$$\tilde{v}_{\mathrm{bot},vx}^{(0)} + i\Gamma_0 \tilde{v}_{\mathrm{bot},vz}^{(0)}/(kc^{(0)}) = 0. \tag{43}$$

It should be noted that the inviscid normal and tangential velocities $\tilde{v}_{oz}$ and $\tilde{v}_{ox}$ do not appear in the above equation, since they are, respectively, $O(\delta)$ and $O(\delta^2)$ smaller than the viscous normal and tangential velocities $\tilde{v}_{\mathrm{bot},vz}$ and $\tilde{v}_{\mathrm{bot},vx}$ [see (26) and (27)]. The generalized Airy function solutions determined (A12) and (A13) for the viscous wall layer quantities $\tilde{v}_{\mathrm{bot},vx}^{(0)}$ and $\tilde{v}_{\mathrm{bot},vz}^{(0)}$ are substituted in the above characteristic equation. It can be readily verified that the above equation reduces to

$$\mathrm{Ai}(y_{\mathrm{wall}}, -1) = 0, \tag{44}$$

where $y_{\mathrm{wall}} = (ik)^{1/3}(-c^{(0)}/\Gamma_0)$ is the value of the variable y (A6) evaluated at the fluid-wall interface $\xi = 0$. It can be
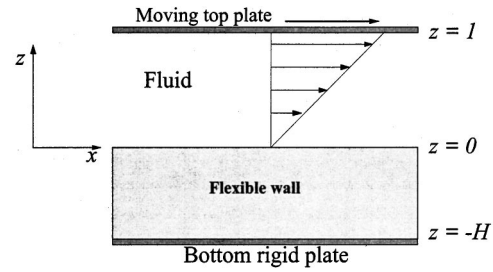

FIG. 4. Schematic diagram showing the configuration and coordinate system considered in Sec. III.

verified that there are multiple solutions to the characteristic equation $\mathrm{Ai}(y_{\mathrm{wall}}, -1) = 0$, and all these solutions are negative real quantities for y_{wall}. This implies that all these solutions correspond to $c^{(0)}$ with negative imaginary parts, indicating that the flow is stable. Thus the present asymptotic analysis shows that wall modes in Couette flow past a spring-backed plate are stable in the limit of high Reynolds number in the absence of tangential wall motion in the plate membrane.

III. WALL MODES IN COUETTE FLOW PAST A VISCOELASTIC SOLID

In this section, an asymptotic analysis is carried out in the limit of high Reynolds number for the case of stability of Couette flow past a viscoelastic continuum. Kumaran et al.[22] carried out a stability analysis for this system in the zero Reynolds number limit, and found the flow to be unstable. Srivatsan and Kumaran[1] numerically continued this zero Reynolds number instability and showed that the zero Reynolds number instability continues to intermediate and high Reynolds number. The system consists of a Newtonian fluid of density ρ, viscosity η, and thickness R (occupying the region $0 < z^* < R$), flowing past a viscoelastic material of finite thickness HR (occupying the region $-HR < z^* < 0$ in the unperturbed state) with shear modulus G and viscosity η_g. A schematic of the configuration is shown in Fig. 4. Here, quantities with a superscript * are dimensional, and quantities without the superscript are dimensionless unless stated otherwise. The fluid is sheared at the top boundary $z^* = R$ with a velocity V, and the base flow velocity profile is the Couette flow profile which is linear in z^*. The wall medium is at rest in the unperturbed base state. The velocities are scaled by $(G/\rho)^{1/2}$, time is scaled by $(\rho R^2/G)^{1/2}$, lengths by R, and the pressure in the fluid and the wall is scaled by G. The ratio of wall-to-fluid viscosities is denoted by $\eta_r = \eta_g/\eta$. As in the previous studies of Refs. 1 and 22, the wall material is assumed to be an incompressible viscoelastic continuum, and the dynamics of the medium is described by a displacement field u_i which represents the displacement of material points from their steady state positions due to the stresses at the surface. The incompressibility condition and the nondimensional momentum balance are given by

$$\partial_i u_i = 0, \quad \partial_t^2 u_i = -\partial_i p_g + \partial_j^2 u_i + \eta_r \partial_j^2 \partial_t u_i, \tag{45}$$

where $\eta_r = \eta_g/\eta$ is the ratio of wall-to-fluid viscosities, and p_g is the pressure in the gel. For simplicity, the density of the

wall material is set to be the same as that of the fluid in the present study. The nondimensional stress tensor in the wall medium consists of an elastic part as well as a viscous part: $\sigma_{ij} = -p_g \delta_{ij} + (\partial_i u_j + \partial_j u_i) + \eta_r \partial_t (\partial_i u_j + \partial_j u_i)$.

The governing equations in the fluid and the scalings for various quantities in the viscous wall layer are the same as that used in the preceding section (Sec. II) for Couette flow past a spring-backed wall [see Eqs. (14)–(16)], except for the difference that the nondimensional top plate velocity Γ in the present section is defined as $\Gamma = (\rho V^2/G)^{1/2}$. The ensuing analysis is qualitatively similar to that presented in Ref. 17, and hence only the important steps are presented here; details can be found in Ref. 17. The solutions for the wall layer velocities provided in the preceding section (A12), for Couette flow past a spring-backed plate carry over in this section except for the change in the definition of Γ. In this section, we consider the limit $\Gamma \sim \mathrm{Re}^{1/3}$ since this scaling is required for the viscous shear stresses in the wall layer [estimated as $V\eta/(\mathrm{Re}^{-1/3}R)$] to be balanced by the elastic stresses in the flexible wall [estimated to be $O(G)$]. However, one modification is needed for the inviscid contributions in the present case. Unlike the flow past a spring-backed walls, in the present case, the inviscid fluid velocities $\tilde{v}_{ox}$ and $\tilde{v}_{oz}$ are $O(\delta)$ small compared to the viscous tangential velocity in the bottom wall layer $\tilde{v}_{vx}$. It is shown in Appendix B that this scaling is required for a balance to be achieved in the normal stress continuity condition at the interface (B17). The inviscid contribution to fluid pressure can then be estimated from the inviscid x-momentum equation (20) to be $O(1)$, since $\Gamma = \Gamma_0 \mathrm{Re}^{1/3}$. For future reference, the magnitudes of the inviscid contributions to the velocity and stress fields are given as $\tilde{v}_{ox} \sim \delta$, $\tilde{v}_{oz} \sim \delta$, $\tilde{\tau}_{ozz} \sim \tilde{p}_{of} \sim 1$, $\tilde{\tau}_{wxz} \sim \delta^3$. According to the above estimates, the inviscid contribution to the fluid velocities and pressure are expanded in an asymptotic series

$$\tilde{v}_{oi} = \delta(\tilde{v}_{oi}^{(0)} + \delta\tilde{v}_{oi}^{(1)} + \cdots), \quad \tilde{p}_{of} = (\tilde{p}_{of}^{(0)} + \delta\tilde{p}_{of}^{(1)} + \cdots), \tag{46}$$

where the subscript $i=x,z$. Once this is recognized, the solutions (A20), (A21) for $\tilde{v}_{oz}^{(0)}$ and $\tilde{v}_{ox}^{(0)}$ carry over to the present case. The governing equations are supplemented by boundary conditions at the interface

$$\tilde{v}_z = -ikc\tilde{u}_z, \tag{47}$$

$$\tilde{v}_x + \Gamma\tilde{u}_z = -ikc\tilde{u}_x, \tag{48}$$

$$\mathrm{Re}^{-1}\Gamma(d_z\tilde{v}_x + ik\tilde{v}_z) = (1 - ikc\,\eta_r\Gamma\,\mathrm{Re}^{-1})(d_z\tilde{u}_x + ik\tilde{u}_z), \tag{49}$$

$$-\tilde{p}_f + 2\Gamma\,\mathrm{Re}^{-1}d_z\tilde{v}_z = -\tilde{p}_g + 2(1 - ikc\,\eta_r\Gamma\,\mathrm{Re}^{-1})d_z\tilde{u}_z. \tag{50}$$

Here, (47) and (48) are, respectively, the normal and tangential velocity continuity conditions at the interface, while (49) and (50) are, respectively, the tangential and normal stress continuity conditions. The wall material is assumed to be fixed to the bottom wall, and the displacement field satisfies zero displacement boundary conditions at $z=-H$:

$$\tilde{u}_x = 0, \quad \tilde{u}_z = 0. \tag{51}$$

The scaling of the boundary conditions at the interface [Eqs. (47)–(50)] is discussed in Appendix B of this paper. This Appendix also contains the solutions to the displacement field in the wall medium.

The asymptotic expansions for the various fluid and wall dynamical quantities are substituted in the six boundary conditions (47)–(51), and the resulting set of equations is written in a matrix form as $\mathbf{MC}=0$, where $\mathbf{C}$ is the vector of constants $[A_1,B_1,B_2,B_3,B_4,C_2]$. Here the constants B_i occur in the solution of the wall displacement field (see Appendix B). In order for this system of equations to have nontrivial solutions, we require $\mathrm{Det}[\mathbf{M}]=0$. This gives the characteristic equation, and this equation is expanded in the small parameter δ. The leading order expression of $\mathrm{Det}[\mathbf{M}]$ yields an expression for $c^{(0)}$, and the first correction to $\mathrm{Det}[\mathbf{M}]$ yields an expression for $c^{(1)}$. The results from the leading order characteristic equation reveals that there are multiple solutions to $c^{(0)}$, all of which are real and positive, indicating that the flow is neutrally stable at this level of approximation. The next correction to the wave speed $c^{(1)}$ is then calculated to determine the stability of the system. It should be noted that the tangential velocity continuity condition at the interface and the fluid tangential stresses in the viscous wall layer appear only at the $O(\delta)$ correction to the characteristic equation. The ratio of wall to fluid viscosities η_r is considered to be an $O(1)$ quantity, and hence does not appear at the first correction to the characteristic equation. This calculation indicates that $c^{(1)}$ is a complex quantity, and the imaginary part of $c^{(1)}$ is set to zero to determine the scaled velocity Γ_0 required for unstable modes. Once Γ_0 is obtained, the neutral curve in the Re–Σ plane can be calculated from the definition $\Sigma = (\mathrm{Re}/\Gamma)^2 = (\mathrm{Re}/(\Gamma_0\mathrm{Re}^{1/3}))^2$. It should be noted here that Σ is a nondimensional parameter characterizing the elasticity of the wall, and it is independent of the flow parameters. This implies that $\mathrm{Re}=\Gamma_0^{3/2}\Sigma^{3/4}$. For each of the multiple solutions $c^{(0)}$, there exists an associated Γ_0, and when $\Gamma > \Gamma_0 \mathrm{Re}^{1/3}$, the flow is unstable. In a previous numerical study, Srivatsan and Kumaran[1] continued the low Reynolds number viscous instability of Couette flow past a flexible surface[22] to the intermediate and high Reynolds number regime. Comparison of the present high-Re asymptotic results with the numerical results of Ref. 1 indicates that the lowest harmonic, i.e., the $c^{(0)}$ with the lowest magnitude and the associated Γ_0 of the asymptotic analysis corresponds to the results of Ref. 1. Figure 5 shows the comparison of the present asymptotic results with the numerical results of Ref. 1, and this figure shows that the numerical results are captured accurately by the present asymptotic analysis. Thus the present asymptotic analysis shows that (i) wall modes are unstable in Couette flow past a viscoelastic medium, and (ii) the numerical continuation of viscous modes[22] to the intermediate Reynolds number[1] regime in Couette flow also leads to the high Reynolds number wall modes.

It is instructive to examine the eigenfunctions of the neutral modes obtained from the full numerical solution, in order to verify whether the scaling assumptions made in the asymptotic analysis for the fluid velocities and wall displacements are consistent with the numerical solution. The eigen-
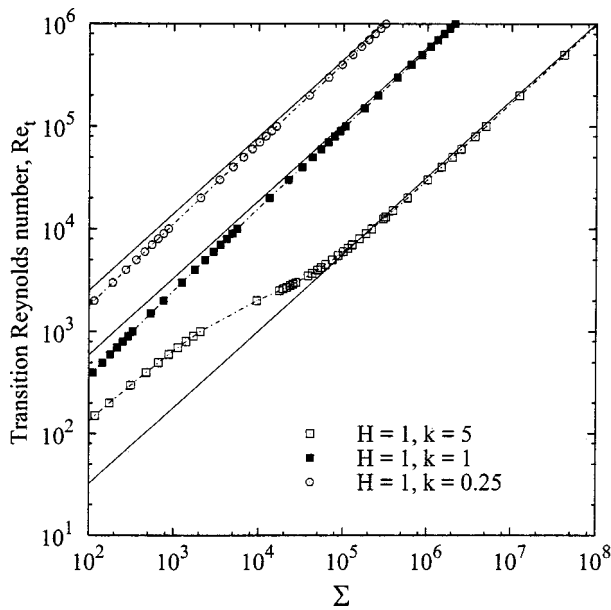
FIG. 5. Comparison of the asymptotic results (solid lines) obtained from the present analysis with the numerical results (dotted lines with symbols) of Ref. 1 for continuation of viscous modes in Couette flow past a flexible surface. $\eta_r = 0$ for all the cases plotted.

FIG. 7. Variation of the absolute value of displacement field in the wall material with Reynolds number Re for Couette flow past a viscoelastic surface: Data from full numerical solution for $H=1$, $k=1$, $\eta_r=0$. The dotted line is the reference straight line with slope $-1/3$.

functions are calculated using the normalization condition that the absolute value of the $\tilde{v}_z$ eigenfunction at the fluid-wall interface satisfies $|\tilde{v}_z|_{z=0} = \sqrt{2}\,\mathrm{Re}^{-1/3}$. Figure 6 shows the variation of various dynamical quantities in the fluid evaluated at $z=0$ with the Reynolds number. By construction, $|\tilde{v}_z|_{z=0}$ scales as $\mathrm{Re}^{-1/3}$ (25). The figure shows that $|\tilde{v}_x|$ is an $O(1)$ quantity [compare with the asymptotic expansion (25)], and $|d_z\tilde{v}_x|$ indeed scales as $\mathrm{Re}^{1/3}$ as was anticipated in the asymptotic analysis. Thus, the results from the full nu-
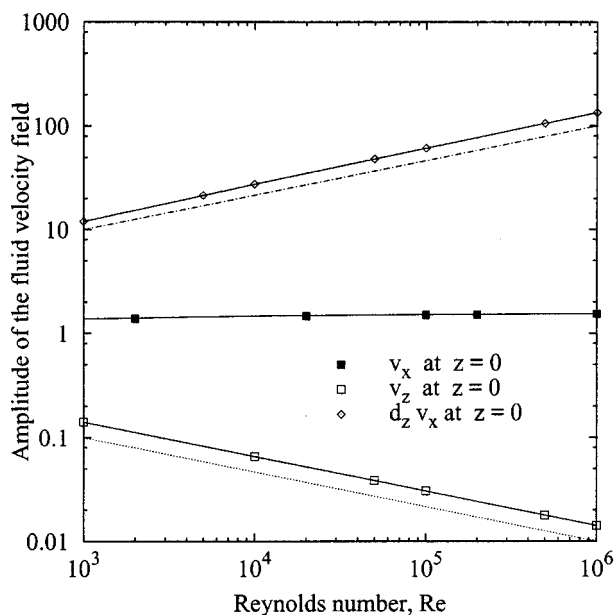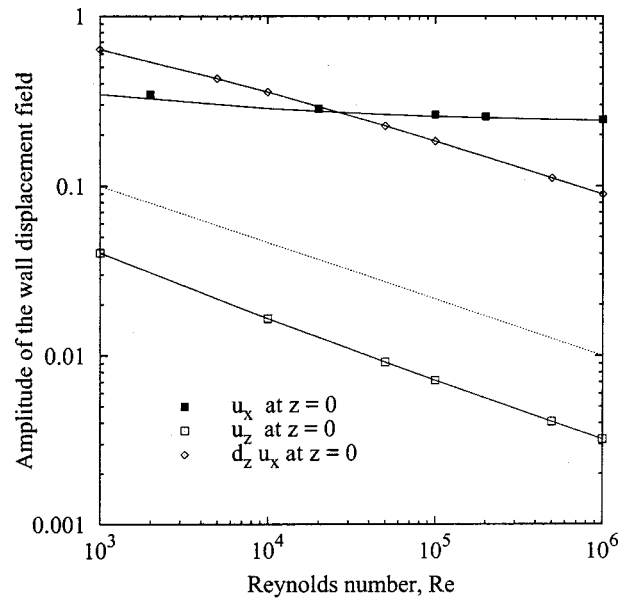

FIG. 6. Variation of the absolute value of velocity field in the fluid with Reynolds number Re in Couette flow past a viscoelastic medium: Data from full numerical solution for $H=1$, $k=1$, $\eta_r=0$. The two dotted lines are reference lines with slopes $-1/3$ and $1/3$.

merical solution for the eigenfunctions of various dynamical quantities in the fluid are consistent with the scaling assumptions made in the asymptotic analysis. Figure 7 shows the variation of the wall displacement field with Re. This figure clearly shows that $|\tilde{u}_z|_{z=0}$ scales as $O(\mathrm{Re}^{-1/3})$. This numerical result is in agreement with the scaling assumptions made in the asymptotic analysis [see Eq. (B6)]. Moreover, as anticipated in the asymptotic analysis, $|\tilde{u}_x|$ is $O(1)$ at $z=0$ [see Eq. (B4)]. Importantly, as shown in the figure, even though $|\tilde{u}_x|$ is $O(1)$ at $z=0$, $|d_z\tilde{u}_x|$ scales as $O(\mathrm{Re}^{-1/3})$ at the interface. This result is again consistent with the outcome of the asymptotic analysis, which indicated that the tangential stresses of the wall at the interface is zero to leading order [see Eq. (B14)], and the next correction to the tangential stresses at the interface is $O(\mathrm{Re}^{-1/3})$ [see Eq. (B13)]. Therefore, the results for eigenfunctions from the full numerical solution are consistent with the scaling assumptions of the asymptotic analysis. Figure 8 shows the variation of the thickness of the wall layer δ with the Reynolds number. The wall layer thickness may be estimated by computing the ratio $\tilde{v}_x/d_z\tilde{v}_x$ at $z=0$ from the full numerical solution. As Fig. 8 shows, the wall layer thickness δ decreases as $\mathrm{Re}^{-1/3}$ in the limit of large Re as predicted by the asymptotic analysis, and this shows that the numerically observed modes are indeed the wall modes. Figures 9 and 10 show the variation of $|\tilde{v}_z|$ and $|\tilde{v}_x|$ in the fluid with z, and here the eigenfunctions are calculated subject to the normalization condition that $|\tilde{v}_z| = \sqrt{2}$ at $z=0$. These figures show that the velocities are large very close to the wall ($z=0$), and there is a small region near the wall where the fluid velocity varies rapidly. Both these observations indicate that the numerical eigenfunctions clearly exhibit the behavior that is characteristic of wall modes.
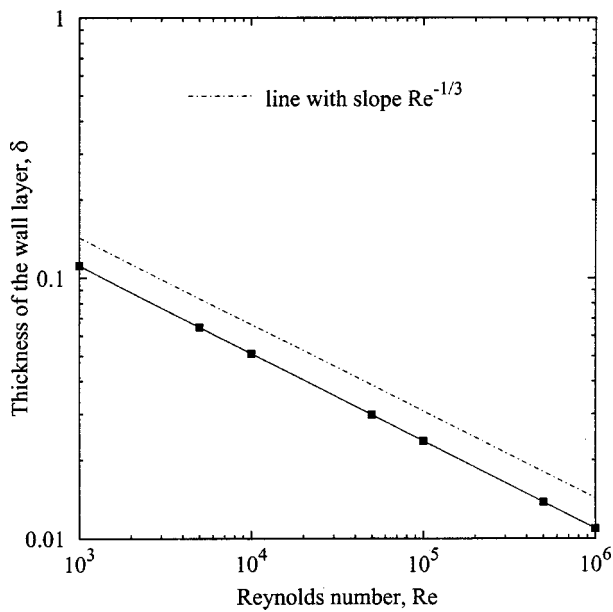
FIG. 8. Variation of the thickness of the wall layer δ with Reynolds number Re for the Couette flow past a viscoelastic medium: Data (symbols) from full numerical solution for $H=1$, $k=1$, $\eta_r=0$.

IV. CONCLUDING REMARKS

The stability of wall modes in fluid flow past a flexible surface is analyzed using a combination of asymptotic and numerical methods. In order to demonstrate that the present instability is not specific to the wall model used, two different wall models are used to determine the stability of Couette flow past a flexible surface. In the first model, the flexible wall is modelled as a spring-backed, plate-membrane-type wall, while in the second model the flexible wall is considered to be an incompressible viscoelastic solid of finite thickness. It is shown that if the spring-backed plate membrane executes only normal wall motion, the high Reynolds number wall modes are stable. However, if tangential wall motion is introduced in the spring-backed membrane wall, the wall modes are shown to become unstable in the high Reynolds number limit. This instability predicted by the asymptotic analysis was subsequently captured by a numerical solution of the full equations governing the stability.
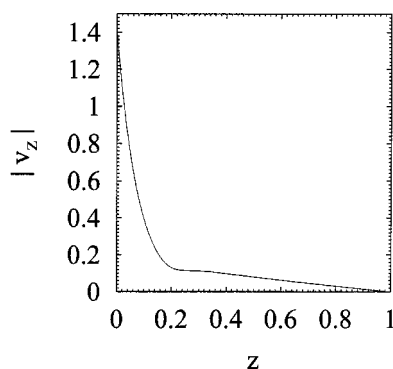

FIG. 9. The absolute value of the $\bar{v}_z$ eigenfunction obtained from the full numerical calculation showing that the variation of the fluid velocity is confined to a small region near the wall: Re=3×10^3, $H=1$, $k=1$, $\eta_r=0$.
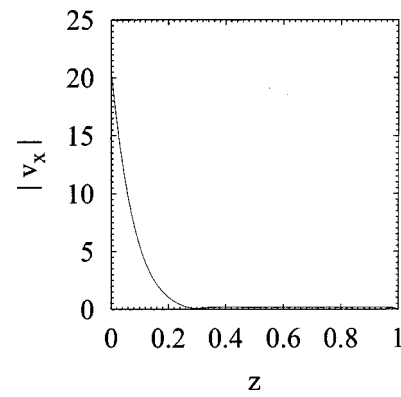

FIG. 10. The absolute value of the $\bar{v}_x$ eigenfunction obtained from the full numerical calculation showing that the variation of the fluid velocity is confined to a small region near the wall: Re=3×10^3, $H=1$, $k=1$, $\eta_r=0$.

Thus, the present study shows that the presence of tangential wall motion in the flexible medium can give rise to a qualitatively new instability in the limit of high Reynolds number where the viscous stresses in the fluid are confined within a thin layer of thickness $O(\text{Re}^{-1/3})$ near the flexible wall, and these instabilities are absent in the case flexible wall models which assume only purely normal wall motion. A similar asymptotic analysis for the Couette flow past a viscoelastic wall of finite thickness shows that the flow is unstable in the limit of high Reynolds number, and the present asymptotic results show that the earlier numerical results of Ref. 1 are indeed the wall modes analyzed in the present study. The asymptotic analysis of wall modes in fluid flow past spring-backed walls further shows that the high-Re wall mode instability analyzed in this paper is really independent of the actual details of the flow profile, and the instability just depends on the fact that the base flow should be zero at the wall, and should have a finite velocity gradient at the wall. Since most of the commonly encountered shear flows such as the Couette flow, plane-Poiseuille flow and the Blasius boundary layer flow satisfy this criterion, the high-Re wall mode instability is expected to exist for all these flows past flexible surfaces.

APPENDIX A

In this appendix, the details of the asymptotic analysis of the fluid governing equations are provided, and the solution for the fluid velocity field in the outer and wall layers are derived.

The asymptotic expansions [Eqs. (24) and (25)] for the various quantities and derivatives are substituted in the governing equations in the fluid. The scaled continuity equation (14) in the wall layer is given by

$$d_\xi \tilde{v}^{(0)}_{\text{bot},vz} + ik\tilde{v}^{(0)}_{\text{bot},vx}=0. \tag{A1}$$

The x-momentum equation (15), then transforms in the wall layer as follows:

$$ik\left[\delta\xi - \mathrm{Re}^{-1/3}\frac{c^{(0)}}{\Gamma_0}\right]\tilde{v}_{\mathrm{bot},vx}^{(0)} + \delta\tilde{u}_{\mathrm{bot},vz}^{(0)}$$

$$= -ik\frac{\tilde{p}_{\mathrm{bot},vf}}{\mathrm{Re}^{1/3}\Gamma_0} + \left[\frac{\delta^{-2}}{\mathrm{Re}}d_\xi^2\tilde{v}_{\mathrm{bot},vx}^{(0)}\right]. \tag{A2}$$

In the above equation, in order to achieve a balance between the inertial term (the term in the square brackets on the left-hand side) and the viscous term (the term in the square brackets on the right-hand side), the small parameter δ should scale as $\delta \sim \mathrm{Re}^{-1/3}$. Without loss of generality, the small parameter δ can be defined as $\delta = \mathrm{Re}^{-1/3}$. In the above equation, in order for the pressure in the wall layer to be of the same magnitude as the other terms, we require $\tilde{p}_{\mathrm{bot},vf} \sim O(1)$ and hence $\tilde{p}_{\mathrm{bot},vf}$ is expanded as $\tilde{p}_{\mathrm{bot},vf} = \tilde{p}_{\mathrm{bot},vf}^{(0)} + \cdots$. The scaled x-momentum equation in the wall layer, to leading order in the small parameter δ, is given by

$$ik\left[\xi - \frac{c^{(0)}}{\Gamma_0}\right]\tilde{v}_{\mathrm{bot},vx}^{(0)} + \tilde{v}_{\mathrm{bot},vz}^{(0)} = -ik\frac{\tilde{p}_{\mathrm{bot},vf}^{(0)}}{\Gamma_0} + d_\xi^2\tilde{v}_{\mathrm{bot},vx}^{(0)}. \tag{A3}$$

The unscaled z-momentum equation (16) can be scaled similarly to obtain the following equation:

$$\delta^2 ik\left[\xi - \frac{c^{(0)}}{\Gamma_0}\right]\tilde{v}_{\mathrm{bot},vx}^{(0)} = -\delta^{-1}d_\xi\tilde{p}_{\mathrm{bot},vf}^{(0)} + \delta^2 d_\xi^2\tilde{v}_{\mathrm{bot},vz}^{(0)}. \tag{A4}$$

The above equation yields, to leading order in δ, $d_\xi\tilde{p}_{\mathrm{bot},vf}^{(0)} = 0$. The equations (A1) and (A3) can be combined along with the condition $d_\xi\tilde{p}_{\mathrm{bot},vf}^{(0)} = 0$, to yield a single differential equation for $\tilde{v}_{\mathrm{bot},vx}^{(0)}$,

$$\left[d_\xi^2 - ik\left(\xi - \frac{c^{(0)}}{\Gamma_0}\right)\right]d_\xi^2\tilde{v}_{\mathrm{bot},vz}^{(0)} = 0. \tag{A5}$$

It is convenient to define another variable y as

$$y = (ik)^{1/3}[-c^{(0)}/\Gamma_0 + \xi], \tag{A6}$$

and the general solution of Eq. (A5) in terms of this new variable is given by

$$\tilde{v}_{\mathrm{bot},vz}^{(0)} = C_0 + C_1\xi + C_2(y\,\mathrm{Ai}(y,1) - \mathrm{Ai}(y,-1))$$

$$+ C_3(y\,\mathrm{Bi}(y,1) - \mathrm{Bi}(y,-1)), \tag{A7}$$

$$\tilde{v}_{\mathrm{bot},vx}^{(0)} = C_1 + C_2\,\mathrm{Ai}(y,1) + C_3\,\mathrm{Bi}(y,1). \tag{A8}$$

Here $\mathrm{Ai}(y,1)$ and $\mathrm{Bi}(y,1)$ are the generalized Airy functions[18]

$$\mathrm{Ai}(y,1) = \int_\infty^y dy\,\mathrm{Ai}(y), \quad \mathrm{Ai}(y,-1) = d_y\,\mathrm{Ai}(y), \tag{A9}$$

$$\mathrm{Bi}(y,1) = \int_\infty^y dy\,\mathrm{Bi}(y), \quad \mathrm{Bi}(y,-1) = d_y\,\mathrm{Bi}(y), \tag{A10}$$

and $\mathrm{Ai}(y)$ and $\mathrm{Bi}(y)$ are the Airy functions which are the solutions of the Airy equation $(d_y^2 + y)\psi(y) = 0$. Two of the linearly independent solutions C_0 and $C_1\xi$ in (A7) are just the inviscid solutions, since these solutions are obtained by setting $d_\xi^2\tilde{v}_{\mathrm{bot},vz}^{(0)} = 0$ in (A5). This can alternatively be veri-

fied by expanding the solution (19) to the inviscid operator $\mathcal{L}_o\tilde{v}_{oz} = 0$. Substituting $z = \delta\xi$ in (19), and expanding to $O(\delta)$ yields

$$\tilde{v}_{oz} = (A_1 + A_2) + (A_1 - A_2)\delta k\xi. \tag{A11}$$

Therefore, we set $C_0 = C_1 = 0$ in (A7).

The Airy functions $\mathrm{Ai}(y,p)$ are convergent in the limit $\xi \to \infty$ only for $(-\pi/3) < \mathrm{Arg}(\xi) < (\pi/3)$, and so it is necessary to choose $\mathrm{Arg}(i^{1/3}) = \pi/6$ in (A6). In this domain, the Airy function $\mathrm{Bi}(y,p)$ diverges, and so we require that $C_3 = 0$. As a result, the solution for the velocities and pressure in the bottom wall layer is given by

$$\tilde{v}_{\mathrm{bot},vz}^{(0)} = -C_2(ik)^{2/3}[y\,\mathrm{Ai}(y,1) - \mathrm{Ai}(y,-1)], \tag{A12}$$

$$\tilde{v}_{\mathrm{bot},vx}^{(0)} = C_2\,\mathrm{Ai}(y,1), \quad \tilde{p}_{\mathrm{bot},vf}^{(0)} = 0, \tag{A13}$$

where the constant C_2 has to be determined from the boundary conditions at the interface $z = 0$.

A similar rescaling procedure can be carried out for the viscous layer near $z = 1$ (the top plate, see Fig. 1), and this yields solutions similar to the above equations for the top wall layer

$$\tilde{v}_{\mathrm{top},vz} = -\delta D_2(ik)^{2/3}[y_1\,\mathrm{Ai}(y_1,1) - \mathrm{Ai}(y_1,-1)], \tag{A14}$$

$$\tilde{v}_{\mathrm{top},vx} = D_2\,\mathrm{Ai}(y_1,1), \tag{A15}$$

where y_1 is a new variable similar to the variable y defined for the bottom wall layer in (A6), with ξ in (A6) being replaced by $\zeta \equiv (1-z)\delta^{-1}$. The constant D_2 appearing in the above equation has to be determined using the no-slip boundary condition at the rigid surface at $z = 1$. It can be readily verified that the viscous solution in the top wall layer merely serves to satisfy the (no-slip) tangential velocity boundary condition at the top rigid wall, and since this viscous solution decays away from the top wall, it does not appear in the boundary conditions at the fluid wall interface at $z = 0$.

The relative magnitudes of $\tilde{v}_{oz}$ and $\tilde{v}_{\mathrm{bot},vz}$ are obtained from the boundary conditions at $z = 0$. We have already set $\tilde{v}_{\mathrm{bot},vx} \sim O(1)$, and hence $\tilde{v}_{\mathrm{bot},vz} \sim O(\delta)$. The leading order pressure in the wall layer is zero, and the next dominant contribution to the fluid pressure in the wall layer is obtained from the z-momentum balance (16), and this shows that the next highest contribution is $O(\delta^2)$ smaller than $\tilde{v}_{vx}$. For future reference, the magnitudes of the viscous contribution to the dynamical quantities in the bottom wall layer are

$$\tilde{v}_{\mathrm{bot},vx} \sim 1, \quad \tilde{v}_{\mathrm{bot},vz} \sim \delta, \quad \tilde{\tau}_{\mathrm{bot},vzz} \sim \delta^2, \quad \tilde{\tau}_{\mathrm{bot},vxz} \sim \delta. \tag{A16}$$

It is shown in the main text [Eq. (34)] that in order to achieve a balance between normal stresses in the fluid and the wall material, it is necessary to stipulate that the inviscid contribution fluid pressure $\tilde{p}_{of}$ is $O(\delta)$. The viscous contribution to the fluid pressure (in the wall layer) is $O(\delta^2)$ as shown above, and hence is subdominant compared to the inviscid pressure component $\tilde{p}_{of}$. Since $\tilde{p}_{of} \sim \delta$, the inviscid velocity $\tilde{v}_{oz}$ should scale as $\tilde{v}_{oz} \sim \delta^2$. This is because the radial and tangential inviscid velocities $\tilde{v}_{oz}$ and $\tilde{v}_{ox}$ are of the same order [as can be inferred from the continuity equation

(20)], and from (21), the inviscid tangential velocity scales as $\tilde{v}_{ox} \sim \tilde{p}_{of}/\Gamma \sim \delta^2$. For future reference, the magnitudes of the inviscid velocity and stress fields are given below

$$\tilde{v}_{ox} \sim \delta^2, \quad \tilde{v}_{oz} \sim \delta^2, \quad \tilde{\tau}_{ozz} \sim \tilde{p}_{of} \sim \delta, \quad \tilde{\tau}_{wxz} \sim \delta^3. \tag{A17}$$

According to the above estimates, the inviscid velocities and pressure are expanded in an asymptotic series,

$$\tilde{v}_{oz} = \delta^2(\tilde{v}_{oz}^{(0)} + \delta\tilde{v}_{oz}^{(1)} + \cdots),$$

$$\tilde{v}_{ox} = \delta^2(\tilde{v}_{ox}^{(0)} + \delta\tilde{v}_{ox}^{(1)} + \cdots),$$

$$\tilde{p}_{of} = \delta(\tilde{p}_{of}^{(0)} + \delta\tilde{p}_{of}^{(1)} + \cdots). \tag{A18}$$

The leading order inviscid velocity field was already solved in (19),

$$\tilde{v}_{oz}^{(0)} = A_1 \exp[kz] + A_2 \exp[-kz]. \tag{A19}$$

One of the constants (say A_2) in the above equation can be eliminated using the condition at the top boundary $\tilde{v}_{oz} = 0$ at $z = 1$. Note that the zero normal velocity boundary condition at the top plate is $\tilde{v}_{oz} + \tilde{v}_{top,vz} = 0$, but this reduces to $\tilde{v}_{oz} = 0$ at $z = 1$, since $\tilde{v}_{top,vz} \sim \delta\tilde{v}_{oz}$. This is because, $\tilde{v}_{ox} \sim \tilde{v}_{top,vx}$ in order to satisfy the tangential no-slip condition at the top rigid plate, and since $\tilde{v}_{ox} \sim \tilde{v}_{oz}$ and $\tilde{v}_{top,vz} \sim \delta\tilde{v}_{top,vx}$, we have $\tilde{v}_{top,vz} \sim \delta\tilde{v}_{oz}$. Therefore, the inviscid velocity field in the fluid is given by

$$\tilde{v}_{oz}^{(0)} = A_1(\exp[kz] - \exp[(2-z)k]), \tag{A20}$$

and the constant A_1 has to be determined from the boundary condition at the fluid-wall interface. The expressions for the tangential velocity $\tilde{v}_{bot,vx}^{(0)}$ and the inviscid fluid pressure $\tilde{p}_{of}$ can be determined from Eqs. (20) and (21). It is easily verified that the solution for the first correction to the inviscid velocity field is identical to the leading-order velocity field, and therefore we can set $\tilde{v}_{oz}^{(1)} = 0$ without loss of generality. The first correction to the inviscid contribution to the fluid pressure can be obtained from the first correction to the x-momentum equation (21),

$$\tilde{v}_{oz}^{(1)} = 0, \quad \tilde{v}_{ox}^{(1)} = 0, \quad \tilde{p}_{of}^{(1)} = c^{(0)}\tilde{v}_{ox}^{(0)}. \tag{A21}$$

APPENDIX B

The scaling of the boundary conditions at the interface (47)–(50) is discussed in this appendix. The solutions for the leading order and first correction to the displacement field in the wall medium are also provided here. The normal velocity continuity condition (47) takes the following form:

$$\delta(\tilde{v}_{oz}^{(0)} + \tilde{v}_{bot,vz}^{(0)}) = -ikc\tilde{u}_z. \tag{B1}$$

Since $c \sim O(1)$ and the left-hand side in the above equation is $O(\delta)$, the above equation indicates that $\tilde{u}_z$ at $z = 0$ is $O(\delta)$. The tangential velocity condition (48) yields

$$\tilde{v}_{bot,vx}^{(0)} + \delta^{-1}\Gamma_0\tilde{u}_z = -ikc\tilde{u}_x. \tag{B2}$$

The left-hand side of the above equation is $O(1)$ for the following reason: $\tilde{v}_{bot,vx}$ is $O(1)$ and $\delta^{-1}\tilde{u}_z$ is $O(1)$ since $\tilde{u}_z$ at $z = 0$ is $O(\delta)$. There are two ways to scale the displacement field in the wall medium. As mentioned before, $\tilde{u}_z$ at

$z = 0$ is $O(\delta)$. So, one possibility is to assume $\tilde{u}_z \sim O(\delta)$ throughout the domain of the wall material. Then the tangential displacement in the wall $\tilde{u}_x \sim O(\delta)$, since in the bulk of the wall medium $\tilde{u}_x \sim \tilde{u}_z$, according to the continuity equation in the wall medium (B19). When $\tilde{u}_x \sim O(\delta)$ in the wall material, the tangential velocity condition (B2) becomes, to leading order

$$\tilde{v}_{bot,vx}^{(0)} + \Gamma_0\tilde{u}_z^{(0)} = 0. \tag{B3}$$

However, as was shown in Sec. II B [see Eqs. (41) and (43)], the above boundary condition yields a characteristic equation $\mathrm{Ai}(y_{wall}, -1) = 0$, and the resulting multiple solutions for $c^{(0)}$ have negative imaginary parts, indicating that the flow is stable for this choice of scalings.

Another possibility to scale the displacement field in the wall is to assume $\tilde{u}_x \sim O(1)$ in (B2) so that the tangential displacement in the wall medium enters the tangential velocity boundary condition at $z = 0$. If $\tilde{u}_x \sim O(1)$, then $\tilde{u}_z \sim O(1)$ in the bulk of the wall medium since according to the continuity equation in the wall, $\tilde{u}_x \sim \tilde{u}_z$. So, the displacement field in the wall medium are expanded in an asymptotic series as

$$\tilde{u}_x = \tilde{u}_x^{(0)} + \delta\tilde{u}_x^{(1)} + \cdots, \quad \tilde{u}_z = \tilde{u}_z^{(0)} + \delta\tilde{u}_z^{(1)} + \cdots. \tag{B4}$$

The above expansions are substituted in the boundary conditions. The normal velocity boundary condition $(\tilde{v}_z = -ikc\tilde{u}_z)$ becomes

$$\delta(\tilde{v}_{oz}^{(0)} + \tilde{v}_{bot,vz}^{(0)}) = -ik(c^{(0)} + \delta c^{(1)} + \cdots)$$
$$\times(\tilde{u}_z^{(0)} + \delta\tilde{u}_z^{(1)} + \cdots). \tag{B5}$$

To leading order in δ, the above boundary condition yields

$$\tilde{u}_z^{(0)} = 0. \tag{B6}$$

The first correction to the normal velocity boundary condition yields

$$(\tilde{v}_{oz}^{(0)} - \tilde{v}_{bot,vz}^{(0)}) = -ik(c^{(0)}\tilde{u}_z^{(1)} + c^{(1)}\tilde{u}_z^{(0)}). \tag{B7}$$

Since $\tilde{u}_z^{(0)} = 0$ at $z = 0$ (B6), the above equation becomes

$$(\tilde{v}_{oz}^{(0)} + \tilde{v}_{bot,vz}^{(0)}) = -ik(c^{(0)}\tilde{u}_z^{(1)}). \tag{B8}$$

The tangential velocity boundary condition $(\tilde{v}_x + \Gamma\tilde{u}_z = -ikc\tilde{u}_x)$ becomes

$$\tilde{v}_{bot,vx}^{(0)} + \delta^{-1}\Gamma_0(\tilde{u}_z^{(0)} + \delta\tilde{u}_z^{(1)} + \cdots)$$
$$= -ik(c^{(0)} + \delta c^{(1)} + \cdots)(\tilde{u}_x^{(0)} + \tilde{u}_x^{(1)} + \cdots). \tag{B9}$$

To leading order in δ, the above equation yields

$$\tilde{u}_z^{(0)} = 0, \tag{B10}$$

which is identical to what was obtained (B6) to leading order from the normal velocity boundary condition. The first correction to (B9) is given by

$$\tilde{v}_{bot,vx}^{(0)} + \Gamma_0\tilde{u}_z^{(1)} = -ikc^{(0)}\tilde{u}_x^{(0)}. \tag{B11}$$

It should be noted here that the tangential velocity in the wall layer appears only in the first correction to the tangential velocity continuity. The unscaled tangential stress condition at the interface is given by

$$\mathrm{Re}^{-1}\,\Gamma[d_z\tilde{v}_x+ik\tilde{v}_z]=(1-ikc\,\eta_r\Gamma\,\mathrm{Re}^{-1})[d_z\tilde{u}_x+ik\tilde{u}_z].$$
(B12)

On using the scalings for various quantities in the above equation, we obtain

$$\Gamma_0\delta(d_\xi\tilde{v}^{(0)}_{\mathrm{bot},vx}+\delta^2 ik\tilde{v}^{(0)}_{\mathrm{bot},vz})$$
$$=(1-ikc\,\eta_r\Gamma_0\delta^2)[(d_z\tilde{u}^{(0)}_x+ik\tilde{u}^{(0)}_z)$$
$$+\delta(d_z\tilde{u}^{(1)}_x+ik\tilde{u}^{(1)}_z)].$$
(B13)

To leading order, the above equation yields

$$(d_z\tilde{u}^{(0)}_x+ik\tilde{u}^{(0)}_z)=0.$$
(B14)

The first correction to (B13) is obtained as

$$\Gamma_0[d_\xi\tilde{v}^{(0)}_{\mathrm{bot},vx}]=(d_z\tilde{u}^{(1)}_x+ik\tilde{u}^{(1)}_z).$$
(B15)

The above equations show that the tangential stresses in the wall layer appears only in the first correction. The unscaled normal stress condition at the interface is given by

$$-\tilde{p}_f+2\,\mathrm{Re}^{-1}\,\Gamma\,d_z\tilde{v}_z$$
$$=-\tilde{p}_g+2(1-ikc\,\eta_r\Gamma\,\mathrm{Re}^{-1})d_z\tilde{u}_z.$$
(B16)

As discussed earlier, $\tilde{p}_f\sim O(1)$ to leading order. The pressure in the wall medium $\tilde{p}_g$ is estimated from the x-momentum equation in the wall (B20), and this reveals that $\tilde{p}_g$ is $O(1)$. On using the scalings for the various quantities, the above boundary condition becomes

$$-(\tilde{p}^{(0)}_f+\delta\tilde{p}^{(1)}_f)+2\Gamma_0\delta^2(d_\xi\tilde{v}^{(0)}_{vz})$$
$$=-(\tilde{p}^{(0)}_g+\delta\tilde{p}^{(1)}_g)+2(1-ikc\,\eta_r\Gamma_0\delta^2)(d_z\tilde{u}^{(0)}_z+\delta d_z\tilde{u}^{(1)}_z).$$
(B17)

The leading order and the first correction equations of the above boundary condition are, respectively, given by

$$-\tilde{p}^{(0)}_f=-\tilde{p}^{(0)}_g+2d_z\tilde{u}^{(0)}_z,\quad -\tilde{p}^{(1)}_f=-\tilde{p}^{(1)}_g+2d_z\tilde{u}^{(1)}_z.$$
(B18)

The governing stability equations for the displacement field in the wall are obtained from (45) after expressing the wall displacement field in terms of normal mode quantities [as in (6)]

$$d_z\tilde{u}_z+ik\tilde{u}_x=0,$$
(B19)

$$-k^2c^2\tilde{u}_x=-ik\tilde{p}_g+(1-ikc\,\eta_r\Gamma\,\mathrm{Re}^{-1})(d_z^2-k^2)\tilde{u}_x,$$
(B20)

$$-k^2c^2\tilde{u}_z=-d_z\tilde{p}_g+(1-ikc\,\eta_r\Gamma\,\mathrm{Re}^{-1})(d_z^2-k^2)\tilde{u}_z,$$
(B21)

where $\eta_r=\eta_g/\eta$ is the ratio of wall to fluid viscosities. On substituting the asymptotic expansions (B4) in Eqs. (B19)–(B21), the equations governing the leading order and first correction to the wall displacement can be obtained, and

these equations can be analytically solved. The solution to the leading order displacement field $\tilde{u}^{(0)}_z$ can be obtained as

$$\tilde{u}^{(0)}_z=B_1\exp[kz]+B_2\exp[\gamma z]+B_3\exp[-kz]$$
$$+B_4\exp[-gz],$$
(B22)

$$\tilde{u}^{(0)}_x=B_1 i\exp[kz]+B_2(i\gamma/k)\exp[\gamma z]$$
$$-iB_3\exp[-kz]-(i\gamma/k)\exp[-\gamma z],$$
(B23)

where $\gamma=k\sqrt{1-(c^{(0)})^2}$. The first correction to the displacement field are given by

$$\tilde{u}^{(1)}_z=B_2(-k^2c^{(0)}c^{(1)}z/g)\exp[\gamma z]$$
$$-B_4 i(-k^2c^{(0)}c^{(1)}z/g)\exp[-\gamma z],$$
(B24)

$$\tilde{u}^{(1)}_x=B_2 i(-k^2c^{(0)}c^{(1)}(1+\gamma z)/(\gamma k))\exp[\gamma z]$$
$$+B_4 i(-k^2c^{(0)}c^{(1)}(-1+\gamma z))\exp[-\gamma z].$$
(B25)

[1] L. Srivatsan and V. Kumaran, "Stability of the interface between a fluid and gel," J. Phys. II **7**, 947 (1997).

[2] P. Krindel and A. Silberberg, "Flow through gel-walled tubes," J. Colloid Interface Sci. **71**, 34 (1979).

[3] V. Kumaran, "Stability of the viscous flow of a fluid through a flexible tube," J. Fluid Mech. **294**, 259 (1995).

[4] V. Kumaran, "Stability of the flow of a fluid through a flexible tube at high Reynolds number," J. Fluid Mech. **302**, 117 (1995).

[5] V. Kumaran, "Stability of fluid flow through a flexible tube at intermediate Reynolds number," J. Fluid Mech. **357**, 123 (1998).

[6] V. Kumaran, "Stability of wall modes in a flexible tube," J. Fluid Mech. **362**, 1 (1998).

[7] V. Shankar and V. Kumaran, "Stability of non-parabolic flow in a flexible tube," J. Fluid Mech. **395**, 211 (1999).

[8] V. Kumaran, "Asymptotic analysis of wall modes in a flexible tube," Eur. Phys. J. B **4**, 519 (1998).

[9] V. Kumaran and R. Muralikrishnan, "Spontaneous growth of fluctuations in the viscous flow of a fluid past a soft interface," Phys. Rev. Lett. **84**, 3310 (2000).

[10] T. B. Benjamin, "Effect of a flexible surface on boundary layer stability," J. Fluid Mech. **9**, 513 (1960).

[11] M. T. Landahl, "On the stability of a laminar incompressible boundary layer over a flexible surface," J. Fluid Mech. **13**, 609 (1962).

[12] P. W. Carpenter and A. D. Garrad, "The hydrodynamic stability of flows over Kramer-type compliant surfaces. Part 1. Tollmien–Schlichting instabilities," J. Fluid Mech. **155**, 465 (1985).

[13] P. W. Carpenter and A. D. Garrad, "The hydrodynamic stability of flows over Kramer-type compliant surfaces. Part 2. Flow induced surface instabilities," J. Fluid Mech. **170**, 199 (1986).

[14] C. Davies and P. W. Carpenter, "Instabilities in a plane channel flow between compliant walls," J. Fluid Mech. **352**, 205 (1997).

[15] P. G. LaRose and J. B. Grotberg, "Flutter and long-wave instabilities in compliant channels conveying developing flows," J. Fluid Mech. **331**, 37 (1997).

[16] P. W. Carpenter and J. S. B. Gajjar, "A general theory for two and three dimensional wall-mode instabilities in boundary layers over isotropic and anisotropic compliant walls," Theor. Comput. Fluid Dyn. **1**, 349 (1990).

[17] V. Shankar and V. Kumaran, "Asymptotic analysis of wall modes in a flexible tube revisited," Eur. Phys. J. B **19**, 607 (2001).

[18] P. Drazin and W. Reid, *Hydrodynamic Stability* (Cambridge University Press, Cambridge, 1981).

[19] P. Carpenter and P. Morris, "The effect of anisotropic wall compliance on

boundary-layer stability and transition," J. Fluid Mech. **218**, 171 (1990).

[20] G. M. Corcos and J. R. Sellars, "On the stability of fully developed pipe flow," J. Fluid Mech. **5**, 97 (1959).

[21] A. E. Gill, "A mechanism for instability of plane Couette flow and of Poiseuille flow in a pipe," J. Fluid Mech. **21**, 145 (1965).

[22] V. Kumaran, G. H. Fredrickson, and P. Pincus, "Flow induced instability of the interface between a fluid and a gel at low Reynolds number," J. Phys. II **4**, 893 (1994).